PAPER

Check for updates

Molecular design towards efficient light-emitting copper(I) halide mononuclear hybrids†

Yi Lv,‡ Jing Yang, ‡ Haibo Li, ‡ Wei Liu * and Gangfeng Ouyang *

In this paper, the structures and optical properties of copper(I) halide mononuclear hybrids have been studied. Three pairs of compounds with different organic ligands have been synthesized by a precursor approach, exhibiting significantly enhanced stability compared to typical copper halide monomers by the formation of stronger Cu–P bonds, proving that copper halide monomer-type hybrid compounds have the potential to be developed into high-performance light-emitting materials.

Introduction

Due to the increasing demand for clean-energy lighting materials, copper halide-based organic–inorganic hybrid structures are a growing family of compounds that are gaining attention for their intriguing luminescent properties.[1–11] This diverse family of compounds warrants more research to better understand their structure–property correlations in order to design new structures with better performance.[12–15] A variety of inorganic building motifs have already been reported for copper halide-based structures, with the most common being a Cu_2X_2 rhomboid dimer, a Cu_4X_4 cubane tetramer, and a $(CuX)_\infty$ staircase chain (Fig. 1a).[16] It is well-understood that the inorganic motifs of these structures determine the overall luminescence mechanism.[17,18] Also, the selection of different organic ligands can tune their optical properties. For copper halide monomers, dimers, and chains, the luminescence mechanism is generally a combination of metal-to-ligand-charge-transfer (MLCT) and halide-to-ligand-charge transfer (XLCT), and for cubane tetramers, their emission is mostly from a cluster-centered (CC) luminescence mechanism.[19,20] Due to the larger ratio of Cu–ligand bonds to Cu/halide atoms in monomer-based compounds, this type of structure should have a very active MCLT process. The reported mononuclear hybrids show extremely high quantum efficiency; however, they are typically extremely unstable, which severely limits their synthesis capabilities and potential applications.[21]

Due to the importance of copper halide hybrid materials, in the past few years, we have been devoted to developing new methods to enhance the stability of them and trying to make them more suitable for practical lighting applications.[22] Under such guidelines, three pairs of novel copper halide molecular mononuclear hybrid materials 0D-CuI(PPh₃)(1-et-im) (**1**, PPh₃ = triphenylphosphine, 1-et-im = 1-ethyl-1*H*-imidazole), 0D-CuI(PPh₃)₂(2-eto-pz) (**2**, 2-eto-pz = 2-ethoxypyrazine) and 0D-CuI(PPh₃)₂(2-pr-pz) (**3**, 2-pr-pz = 2-propylpyrazine) have been synthesized by a precursor approach (Fig. 1b),[23] showing blue, green and yellow emissions, respectively, which proves the optical tunability of these compounds and the universality of the synthetic method. These compounds show high
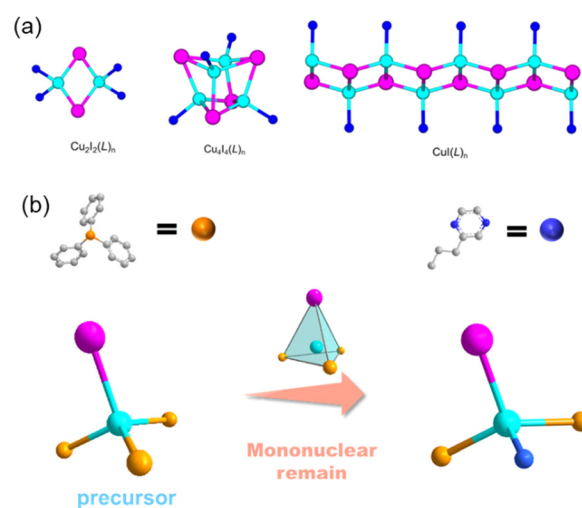
School of Chemical Engineering and Technology, Sun Yat-Sen University, Zhuhai, 519082, China. E-mail: liuwei96@mail.sysu.edu.cn, cesoygf@mail.sysu.edu.cn

Fig. 1 (a) Typical structures of a rhomboid dimer 0D-Cu₂I₂(L)₄, a cubane tetramer 0D-Cu₄I₄(L)₄, and a staircase chain 1D-CuI(L). (b) Scheme of the bottom-up strategy for the mononuclear structure. Cyan balls: Cu, pink balls: I, blue balls: N-ligand, yellow balls: PPh₃.

quantum yields, and enhanced thermal and moisture stability, proving that monomer materials have the potential to be developed into high-performance light-emitting materials.

Experimental

Materials

CuI ($>$99.5%, Aladdin), triphenylphosphine (PPh$_3$, $>$99.0%, Aladdin), 1-ethyl-1H-imidazole (99.76%, Bidepharm), 2-ethoxy-pyrazine (98.0%, Macklin), 2-propylpyrazine (99.96%, Bidepharm), acetonitrile (AR, Macklin), dichloromethane (AR, Macklin), acetone (AR), methanol (AR), and ethanol anhydrous ($>$99.7%).

Preparation of the CuI(PPh$_3$)$_3$ precursor

Monomeric coordination compounds with a 1:3 molar ratio stoichiometry of CuI salt and PPh$_3$ were synthesized utilizing the experimental instructions previously reported.[24] Under sonication, 1 mmol CuI was dispersed in 20 mL acetonitrile, and then 20 mL acetonitrile dissolving 3 mmol PPh$_3$ was dropwise added into the CuI dispersion. After 10 min's sonication, the white powdery CuI(PPh$_3$)$_3$ precursor product was collected by filtration, washed with acetonitrile, and dried under vacuum. The yield is 87% based on Cu.

Synthesis of 0D-CuI(PPh$_3$)$_2$(1-et-im)

The precursor approach was applied for the synthesis of 0D-CuI(PPh$_3$)$_3$ and it was chosen as the precursor. In a typical synthesis, 0D-CuI(PPh$_3$)$_3$ (0.1 g) and 1-et-im (0.1 mL) were added into CH$_2$Cl$_2$/toluene (1:1, v:v) in a closed reaction vial and the reaction mixture was kept at 80 °C for 24 h. Colorless cubic crystals were formed along with a pure phase of power products at the bottom of the vial. They were collected by filtration, washed with ethanol three times and dried in a vacuum oven for 3 h before further characterization (62% yield based on Cu). The following compounds were synthesized in a similar manner unless stated otherwise.

Synthesis of 0D-CuI(PPh$_3$)$_2$(2-eto-pz)

The precursor approach was applied for the synthesis of 0D-CuI(PPh$_3$)$_3$ and it was chosen as the precursor. In a typical synthesis, 0D-CuI(PPh$_3$)$_3$ (0.1 g) and 2-eto-pz (0.1 mL) were added into CH$_2$Cl$_2$/toluene (1:1, v:v) in a closed reaction vial and the reaction mixture was kept at 80 °C for 24 h. Colorless cubic crystals formed along with a pure phase of power products at the bottom of the vial. They were collected by filtration, washed with ethanol three times and dried in a vacuum oven for 3 h before further characterization (67% yield based on Cu).

Synthesis of 0D-CuI(PPh$_3$)$_2$(2-pr-pz)

The synthetic procedure is the same as above except that the N-ligand is 2-pr-pz. Yellowish plate-shaped crystals formed in 24 h (59% yield based on Cu).

Single crystal X-ray diffraction

Single crystal data of compounds **1**–**3** are listed in Table 1. These data can be obtained free of charge from The Cambridge Crystallographic Data Centre via www.ccdc.cam.ac.uk/data_re-quest/cif. The structures were deposited in Cambridge Structural Database (CSD) with numbers 2286691–2286693.

Powder X-ray diffraction (PXRD)

PXRD analyses were carried out on a Rigaku Ultima IV automated diffraction system using Cu Kα radiation (λ = 1.5406 Å). The data were collected at room temperature in a 2θ range of 5–50° with a scan speed of 10° min^{-1}. The operating power was 40 kV/40 mA.

Thermogravimetric (TG) analysis

TG analyses of the coatings were performed on a STA449F3 (NETZSCH). Pure powder samples were loaded into platinum pans and heated with a ramp rate of 10 K min^{-1} from 30 °C to 810 °C.

Photoluminescence (PL) measurements

Photoluminescence (PL) measurements were carried out on an Edinburgh instruments, FS5 spectrophotometer at room temperature. Room temperature PL lifetime decay curves were collected on a LifeSpec II (Edinburgh Instruments).

Optical diffuse reflectance measurements

Optical diffuse reflectance spectra were measured at room temperature on a Shimadzu UV-3600 spectrophotometer. Data

Table 1 Crystallographic data and structural refinement details of the new structures

Compound	0D-CuI(PPh$_3$)$_2$(1-et-im)	0D-CuI(PPh$_3$)$_2$(2-eto-pz)	0D-CuI(PPh$_3$)$_2$(2-pr-pz)
Empirical Formula	C$_{41}$H$_{38}$CuIN$_2$P$_2$	C$_{42}$H$_{38}$CuIN$_2$OP$_2$	C$_{43}$H$_{40}$CuIN$_2$P$_2$
FW	811.11 g mol^{-1}	839.12 g mol^{-1}	837.15 g mol^{-1}
Space Group	$P121/n1$	$P2_1/c$	$P121/c1$
a (Å)	9.4826(3)	9.7312(5)	9.7476(4)
b (Å)	19.3001(5)	36.8870(17)	38.3409(15)
c (Å)	19.8003(6)	11.3310(5)	11.0275(4)
A (°)	90	90	90
B (°)	94.531(3)	115.160(2)°	114.065(2)
γ (°)	90	90	90
V (Å^3)	3612.43(18)	3680.43(31)	3763.12(30)
Z	4	4	4
T (K)	100	283	283

were collected in the wavelength range of 200–800 nm. BaSO$_4$ powder was used as a standard (100% reflectance).

Internal quantum yield measurements

IQY values were measured on a C9920-02 quantum yield measurement system (Hamamatsu Photonics) with a 150 W xenon monochromatic light source and 3.3 inch integrating sphere at room temperature. Samples for internal quantum yield measurements were prepared by spreading fine powder samples evenly on the bottom of a quartz sample holder.

First principles calculation methods

The crystal structure calculations are carried out using the GPU accelerated first principles software package PWmat.[25] We applied the Perdew–Burke–Ernzerhof (PBE)[26] exchange correlation functional with the generalized gradient approximation. All elements in the system are described by the norm-conserving pseudopotentials in the form of SG15 Optimized Norm-Conserving Vanderbilt (ONCV).[27,28] The valence orbitals for each element are listed as Cu(3s, 3p, 3d, 4s), P(3s, 3p), H(1s), C(2s, 2p), N(2s, 2p), O(2s, 2p), Cl(3s, 3p, 3d), Br (4s, 4p), and I(4d, 5s, 5p). The kinetic energy cutoff is at about 952 eV with the force threshold as 0.02 eV Å^{-1} during the structural optimization, and the van der Waals correction is added using Grimme's D3.[29] The k-point sample is under the Monkhorst–Pack[30] scheme with the dimensions of $3 \times 3 \times 1$ given the large dimensions of the crystal single cells. The ligand structural optimization and electronic structure analysis are performed using the *ab initio* software package, BDF,[31–34] implemented in Device Studio, Version 2022B.[35] We performed structural optimization at B3LYP[36–39]/6-31G(d) and evaluated the frontier orbital properties using 6-311++G(3df, 3pd)[40–48] basis sets. The van der Waals correction method is Grimme's D3.[49,50]

Results and discussion

Copper halide monomers with pyridine derivatives are generally synthesized by directly mixing the ligands with copper halides in acetonitrile.[51] These compounds are extremely unstable in air and will completely decompose in a few hours in the air. They are also very sensitive to moisture, since they break down immediately in contact with water. Once the product forms, they must immediately be separated from solution to prevent decomposition and should be kept under vacuum. Moreover, during the reaction, other more stable phases such as dimers, cubane tetramers, or staircase chains may form under the same synthetic conditions. Therefore, rational synthesis of keeping the copper halide mononuclear motif in the products can be achieved by using a monomer precursor 0D-CuI(PPh$_3$)$_3$ as a starting material instead of bulk copper halides. By using the precursor approach, three pairs of luminescent copper halide structures **1**–**3** with a mononuclear core have been obtained. In a typical synthesis, the precursor and the N-ligands were added into a CH$_2$Cl$_2$/toluene (1 : 1, v : v) in a closed reaction vial and the reaction mixture was kept at
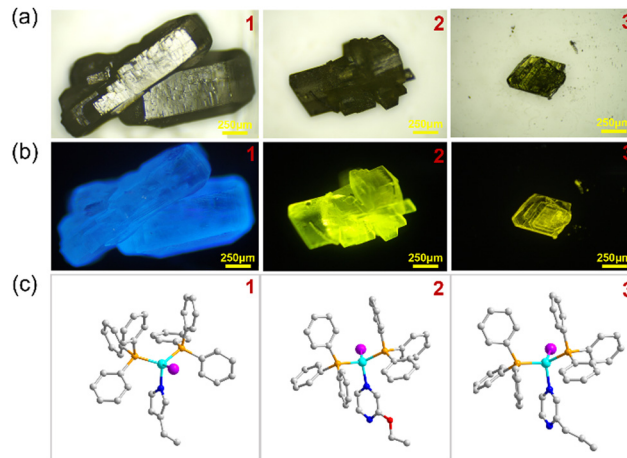

Fig. 2 Images of crystals of compounds **1**–**3** under white light (a) and 365 nm UV light (b), crystal structures of compounds **1**–**3** (c), different colors indicate various element atoms, light blue: Cu; yellow: P; grey: C; purple: I; deep blue: N; red: O.

80 °C for 24 h. Single crystals formed along with a pure phase of power products at the bottom of the vial (Fig. 2). Typically, the direct reaction of copper halide with N-ligands would lead to the formation of hybrid structures with different inorganic modules, such as copper halide staircase chain type, rhomboid dimer type, cubane tetramer type, *etc.* These compounds show different luminescent properties, while structures with discrete inorganic motifs generally show better luminescent efficiency. Also, the Cu–P bond is stronger than the common Cu–N bond, so that structures with PPh$_3$ coordination show improved stability. Therefore, different from the traditional crystallization method, the precursor strategy effectively eliminates the possibility of other types of products. And molecular design principles are proposed here for the synthesis of PPh$_3$-coordinated mononuclear complexes with improved luminescent efficiency and stability.

The crystal structures of compounds **1**–**3** have been determined by single crystal X-ray diffraction (SCXRD). Crystallographic data and structural refinement details have been summarized in Table 1. Compounds **1**–**3** are all 0D molecular clusters with a copper iodide mononuclear core (Fig. 2c and Fig. S1, ESI†). When the N-ligand is added to the reaction mixture, the three PPh$_3$ in the cluster precursor are partially replaced by the N-ligand. The general formula of compounds **1-3** is 0D-CuI(PPh$_3$)$_2$(L) (L = monodentate N-ligands). In those structures, one copper atom is coordinated to one halide atom, two PPh$_3$ molecules and one mono-dentate N-ligand molecule, displaying mononuclear tetrahedral coordination geometry. The phase purity of compounds **1**–**3** is confirmed by powder X-ray diffraction analysis (PXRD, Fig. S2, ESI†). The peak positions of the observed PXRD patterns are in good agreement with those simulated from single crystal X-ray data, indicating that pure phases are obtained and are used for further characterization.

The optical absorption spectra of **1**–**3** were collected at room temperature and their band gaps are estimated from the optical
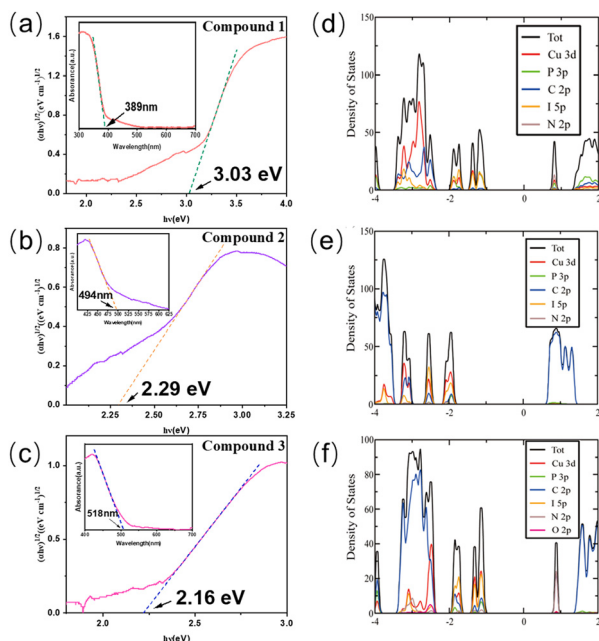
Fig. 3 (a)–(c) The optical diffuse reflectance spectra (inset) and the corresponding Tauc plots of compounds **1–3**, respectively. (d)–(f) Calculated density of states of compounds **1–3**. The total density of states (black); Cu 3d orbitals (red); P 3p orbitals (green); C 2p orbitals (blue); N 2p orbitals (brown); O 2p orbitals (dark pink).

absorption data by the Tauc method (Fig. 3a–c). The absorption edges for compounds **1–3** were found to be 3.03 eV for compound **1**, 2.29 eV for compound **2**, and 2.16 eV for compound **3**, and the results are listed in Table 2. The density functional theory (DFT) methods are used to optimize the ligands and the newly synthesized crystal structures (Fig. 3d–f). The calculation results show that the valence band maximum (VBM) mainly consists of inorganic components (Cu 3d, I 5p orbitals), while the conduction band minimum (CBM) is comprised from the organic ligand (C 2p, N 2p, P 3p orbitals). As ligands with different LUMO energies are incorporated into the structure, the band gap values of the compounds are in agreement with the LUMO energies of the ligands. As for compounds **1–3**, the decreasing trend in their band gap values corresponds to the decreasing ligand LUMO energies, which are −0.471 eV, −1.605 eV, and −1.692 eV for 1-et-im, 2-eto-pz, and 2-pr-pz, respectively. As for tpp-based structures, both the PPh$_3$ and the nitrogen-based ligand contribute to the conduction band, and as a result, the CBM is determined by the combination of the two. The LUMO energy for PPh$_3$ is calculated to be −0.391 eV, higher than the LUMO energies of most of the N-ligands. Therefore, PPh$_3$ acts as a dimensionality controller, since

without PPh$_3$, one dimensional or two dimensional hybrid structures are easy to form using these ligands. Also, PPh$_3$ acts as an optical modulator, tuning the band gaps and luminescence.

The photoluminescence data show that the emission of these compounds is single-band emission, with a full width at half maximum (FWHM) of around 100 nm (Fig. 4a–c). The emission colors range from blue to yellow, spanning the visible light region. Their emission energies are in agreement with their band gap values. Internal quantum yield (IQY) values of these compounds were measured and all of these compounds show IQY higher than 60%. Compounds with ligands of higher LUMO energy have higher quantum yield than those with ligands of lower LUMO energy. One possible reason is that the excited states of lower band gap compounds are usually more stable and would have a longer lifetime, than that of higher band gap ones. This would decrease their quantum yields by allowing more opportunities for non-radiative recombination. It is accepted that metal-to-ligand charge transfer (MLCT) plays an important role in the luminescence mechanism for the monomer, which is in agreement with the DFT calculations. The luminescent decay curves of these three compounds at room temperature are shown in Fig. 4d–f, giving a long lifetime of approximately 8 μs, 24 μs and 23 μs by monoexponential fitting. The photophysical data of compounds **1–3** are summarized in Table 2.

Stability is an important criterion for the evaluation of the performance of lighting materials. Based on our earlier research, we have developed three major strategies for enhancing the stability of copper–halide based structures with discrete inorganic motifs while maintaining their luminescent properties, which have been applied in this work. The approaches include: (I) using a molecular precursor to keep the inorganic motif with ligand exchange to create the desired product; (II) introducing triphenylphosphine molecules into the structures since the Cu–P bonds are more robust compared to Cu–N bonds; (III) replacing the commonly used pyridine (py) derivatives with imidazole (im) derivatives that could form stronger Cu–N bonds. Under these approaches, compounds **1–3** exhibit enhanced thermal stability with decomposition temperature higher than 100 °C (Fig. S3, ESI†). The chemical stability was evaluated by soaking the samples in water. As shown in Fig. S4 (ESI†), compounds **1**, **2** and **3** were selected and were dispersed in water for 7 days. All their structures remain intact, which was proved by PXRD, and their luminescence shows no obvious change after the dispersion. These compounds are air and moisture stable. The photo-stability of the compounds has been evaluated by placing compound **3** under UV irritation in the open air. As shown in Fig. S5a (ESI†),

Table 2 Optical properties and thermal decomposition temperatures of compounds **1–3**

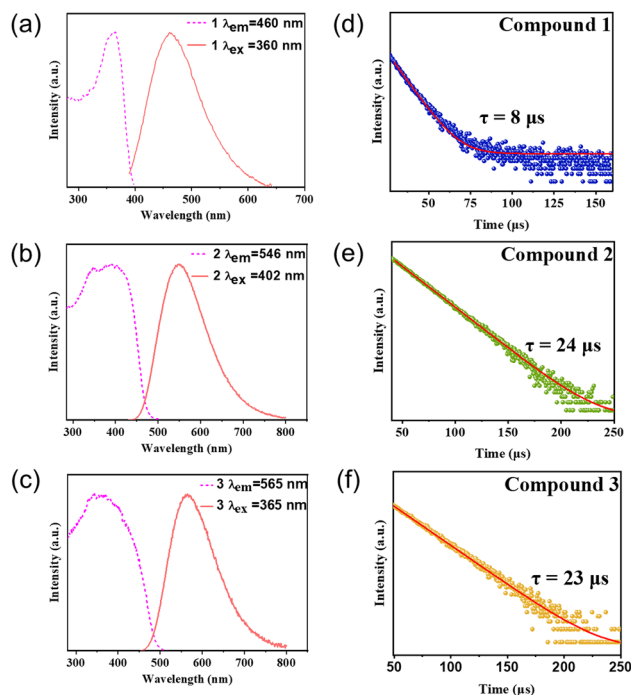| #	Structures	Band gap (eV)	λ_{em} (nm, R.T.)	Emission color	IQY(%)	Decom. Temp. (°C)	CIE (x,y)
1	0D-CuI(tpp)$_2$(1-et-im)	3.03	460	Blue	72	130	(0.183, 0.207)
2	0D-CuI(tpp)$_2$(2-eto-pz)	2.29	546	Yellow-green	69	100	(0.399, 0.529)
3	0D-CuI(tpp)$_2$(2-pr-pz)	2.16	565	Yellow	67	110	(0.450, 0.520)

Fig. 4 (a)–(c) Photoluminescence excitation (dashed lines) and emission (solid lines) spectra of compounds **1**–**3**. (d)–(f) Luminescence decay curves of compounds **1**–**3**.

the IQY drops from 67% to 53%, indicating the moderate stability of these phosphors. Samples left under air for several months retain the structures and the emission intensity (Fig. S5b and c, ESI†). The emission spectrum at elevated temperature has been provided in Fig. S5d (ESI†).

In order to obtain two-component white phosphors, highly emissive compound **1** was selected as the blue-emitting component to blend with yellow-emitting compound **3**. A white phosphor is obtained by grinding the blue phosphor and yellow phosphor with various mass ratios, respectively, and dispersed with water-soluble binder and then coated onto UV chips (3.4 V, 360 nm). PL spectra are displayed in Fig. 5a. Fig. 5b shows the photo image of the coated chips under working conditions, displaying cold white light to warm white light. The
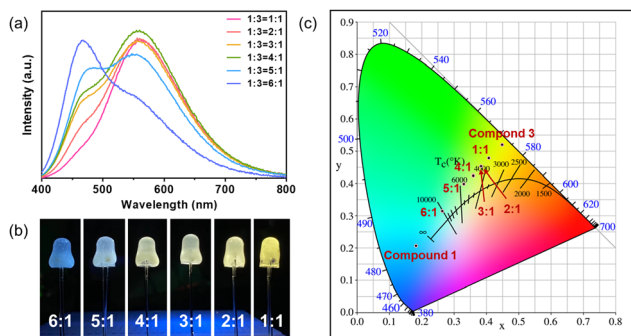

Fig. 5 (a) The emission spectra of the phosphor blends. (b) Photo image of the phosphor-coated LED chips. (c) CIE coordinates of the phosphor blends.

CIE coordinates of the white light blenders are plotted in Fig. 5c. The luminescent efficiency and stability of these compounds have been compared with other reported ones. As shown in Table S1 (ESI†), these compounds show improved stability compared to other copper halide monomers without PPh_3. Their luminescence efficiency is much higher than that of 1D or 2D staircase chain-type structures.

Conclusions

In summary, a series of mononuclear organic–inorganic hybrid structures have been designed and synthesized, displaying the features of high luminescence and improved stability. The use of the 0D-CuI(PPh_3)$_3$ precursor enables the preservation of the mononuclear structure, which also leads to high luminescent efficiency (IQY higher than 60%). The introduction of a rigid precursor increases the decomposition temperature from the original room temperature to higher than 100 °C. The blue component can be ground with the yellow component to obtain white-light-emitting phosphor blends.

Author contributions

Y. L. was responsible for performing all experiments; J. Y. was responsible for the DFT calculations; H. L. was responsible for the characterization of the compounds and the editing of the manuscript; W. L. was responsible for reviewing and editing the manuscript; G. O. was responsible for the supervision of the project, and reviewing and editing the manuscript. All authors have given approval to the final version of the manuscript.

Conflicts of interest

There are no conflicts to declare.

Acknowledgements

Notes and references

1 H. Wang, J.-X. Wang, X. Song, T. He, Y. Zhou, O. Shekhah, L. Gutiérrez-Arzaluz, M. Bayindir, M. Eddaoudi, O. M. Bakr and O. F. Mohammed, *ACS Cent. Sci.*, 2023, **9**, 668–674.

2 W. Liu, Y. Fang and J. Li, *Adv. Funct. Mater.*, 2018, **28**, 1705593.

3 J. Troyano, F. Zamora and S. Delgado, *Chem. Soc. Rev.*, 2021, **50**, 4606–4628.

4 X. Hei, W. Liu, K. Zhu, S. J. Teat, S. Jensen, M. Li, D. M. O'Carroll, K. Wei, K. Tan, M. Cotlet, T. Thonhauser and J. Li, *J. Am. Chem. Soc.*, 2020, **142**, 4242–4253.

5 M. Xie, C. Han, Q. Liang, J. Zhang, G. Xie and H. Xu, *Sci. Adv.*, 2019, **5**, eaav9857.

6 R.-J. Wei, H.-G. Zhou, Z.-Y. Zhang, G.-H. Ning and D. Li, *CCS Chem.*, 2020, **3**, 2045–2053.

7 D. Sun, S. Yuan, H. Wang, H.-F. Lu, S.-Y. Feng and D.-F. Sun, *Chem. Commun.*, 2013, **49**, 6152–6154.

8 Q. Hu, C. Zhang, X. Wu, G. Liang, L. Wang, X. Niu, Z. Wang, W.-D. Si, Y. Han, R. Huang, J. Xiao and D. Sun, *Angew. Chem., Int. Ed.*, 2023, **62**, e202217784.

9 X.-H. Zhao, N.-N. Li, J. Xu, X.-Y. Dong, S. Li and S.-Q. Zang, *Chin. J. Chem.*, 2023, **41**, 1943–1949.

10 B. Zhou, Z. Qi, M. Dai, C. Xing and D. Yan, *Angew. Chem., Int. Ed.*, 2023, **62**, e202309913.

11 B. Zhou and D. Yan, *Adv. Funct. Mater.*, 2023, **33**, 2300735.

12 X. Hei and J. Li, *Chem. Sci.*, 2021, **12**, 3805–3817.

13 K. Zhu, Z. Cheng, S. Rangan, M. Cotlet, J. Du, L. Kasaei, S. J. Teat, W. Liu, Y. Chen, L. C. Feldman, D. M. O'Carroll and J. Li, *ACS Energy Lett.*, 2021, **6**, 2565–2574.

14 B. Zhou and D. Yan, *Sci. Bull.*, 2023, **68**, 469–472.

15 S. Liu, Y. Lin and D. Yan, *Sci. Bull.*, 2022, **67**, 2076–2084.

16 R. Peng, M. Li and D. Li, *Coord. Chem. Rev.*, 2010, **254**, 1–18.

17 Q. Benito, X. F. Le Goff, S. Maron, A. Fargues, A. Garcia, C. Martineau, F. Taulelle, S. Kahlal, T. Gacoin, J.-P. Boilot and S. Perruchas, *J. Am. Chem. Soc.*, 2014, **136**, 11311–11320.

18 H. Araki, K. Tsuge, Y. Sasaki, S. Ishizaka and N. Kitamura, *Inorg. Chem.*, 2005, **44**, 9667–9675.

19 P. C. Ford, E. Cariati and J. Bourassa, *Chem. Rev.*, 1999, **99**, 3625–3648.

20 K. R. Kyle, C. K. Ryu, P. C. Ford and J. A. DiBenedetto, *J. Am. Chem. Soc.*, 1991, **113**, 2954–2965.

21 W. Liu, W. P. Lustig and J. Li, *Energy Chem.*, 2019, **1**, 100008.

22 H. Li, Y. Lv, Z. Zhou, H. Tong, W. Liu and G. Ouyang, *Angew. Chem., Int. Ed.*, 2022, **61**, e202115225.

23 W. Liu, Y. Fang, G. Z. Wei, S. J. Teat, K. Xiong, Z. Hu, W. P. Lustig and J. Li, *J. Am. Chem. Soc.*, 2015, **137**, 9400–9408.

24 P. F. Barron, J. C. Dyason, P. C. Healy, L. M. Engelhardt, C. Pakawatchai, V. A. Patrick and A. H. White, *J. Chem. Soc., Dalton Trans.*, 1987, 1099–1106, DOI: 10.1039/DT9870001099.

25 W. Jia, J. Wang, X. Chi and L.-W. Wang, *Comput. Phys. Commun.*, 2017, **211**, 8–15.

26 J. P. Perdew, K. Burke and M. Ernzerhof, *Phys. Rev. Lett.*, 1996, **77**, 3865–3868.

27 D. R. Hamann, *Phys. Rev. B: Condens. Matter Mater. Phys.*, 2013, **88**, 085117.

28 M. Schlipf and F. Gygi, *Comput. Phys. Commun.*, 2015, **196**, 36–44.

29 S. Grimme, *J. Comput. Chem.*, 2006, **27**, 1787–1799.

30 H. J. Monkhorst and J. D. Pack, *Phys. Rev. B: Solid State*, 1976, **13**, 5188–5192.

31 W. Liu, G. Hong, D. Dai, L. Li and M. Dolg, *Theor. Chem. Acc.*, 1997, **96**, 75–83.

32 W. Liu, F. Wang and L. Li, *J. Theor. Comput. Chem.*, 2003, **02**, 257–272.

33 W. Liu, F. Wang and L. Li, in *Recent Advances in Relativistic Molecular Theory*, ed. K. H. Y. Ishikawa, 2004, vol. 5, pp. 257–282.

34 J. An, Y. Wang, Z. Zhang, J. Zhang, M. Gocyla, R. E. Dunin-Borkowski and F. Wang, *Chin. J. Catal.*, 2020, **41**, 963.

35 Hongzhiwei Technology, Device Studio, Version 2022B, China, https://iresearch.net.cn/cloudSoftware.

36 A. D. Becke, *J. Chem. Phys.*, 1993, **98**, 5648–5652.

37 C. Lee, W. Yang and R. G. Parr, *Phys. Rev. B: Condens. Matter Mater. Phys.*, 1988, **37**, 785–789.

38 P. J. Stephens, F. J. Devlin, C. F. Chabalowski and M. J. Frisch, *J. Phys. Chem.*, 1994, **98**, 11623–11627.

39 S. H. Vosko, L. Wilk and M. Nusair, *Can. J. Phys.*, 1980, **58**, 1200–1211.

40 D. Feller, *J. Comput. Chem.*, 1996, **17**, 1571–1586.

41 B. P. Pritchard, D. Altarawy, B. Didier, T. D. Gibsom and T. L. Windus, *J. Chem. Inf. Model.*, 2019, **59**, 4814–4820.

42 K. L. Schuchardt, B. T. Didier, T. Elsethagen, L. Sun, V. Gurumoorthi, J. Chase, J. Li and T. L. Windus, *J. Chem. Inf. Model.*, 2007, **47**, 1045–1052.

43 M. J. Frisch, J. A. Pople and J. S. Binkley, *J. Chem. Phys.*, 1984, **80**, 3265–3269.

44 T. Clark, J. Chandrasekhar, G. W. Spitznagel and P. V. R. Schleyer, *J. Comput. Chem.*, 1983, **4**, 294–301.

45 M. M. Francl, W. J. Pietro, W. J. Hehre, J. S. Binkley, M. S. Gordon, D. J. DeFrees and J. A. Pople, *J. Chem. Phys.*, 1982, **77**, 3654–3665.

46 R. Krishnan, J. S. Binkley, R. Seeger and J. A. Pople, *J. Chem. Phys.*, 1980, **72**, 650–654.

47 A. D. McLean and G. S. Chandler, *J. Chem. Phys.*, 1980, **72**, 5639–5648.

48 G. W. Spitznagel, T. Clark, P. V. R. Schleyer and W. J. Hehre, *J. Comput. Chem.*, 1987, **8**, 1109–1116.

49 S. Grimme, J. Antony, S. Ehrlich and H. Krieg, *J. Chem. Phys.*, 2010, **132**, 154104.

50 S. Grimme, S. Ehrlich and L. Goerigk, *J. Comput. Chem.*, 2011, **32**, 1456–1465.

51 C. Xu, L. Lu, L. Lv, Y. Li, F. Lin, Y. Yang, F. Lin, C. Luo, D. Luo and W. Liu, *Mol. Cryst. Liq. Cryst.*, 2020, **709**, 54–60.